



**宝钢学术年会**

Baosteel Annual Academic Conference

# 首届宝钢学术年会论文集

第四分册:不锈钢和特殊钢生产工艺及其产品研发

## Baosteel AAC '04 Proceedings

May 27-28, 2004  
Shanghai, China

### **Volume 4** **Stainless Steels** **and other Alloyed Steel Grades** **and Processing**

上海宝钢集团公司

Shanghai Baosteel Group Corporation

# **首届宝钢学术年会论文集**

第四分册: 不锈钢和特殊钢生产工艺及其产品研发

---

## **Baosteel AAC '04 Proceedings**

May 27-28, 2004  
Shanghai, China

### **Volume 4**

**Stainless Steels  
and other Alloyed Steel Grades  
and Processing**

上海宝钢集团公司  
Shanghai Baosteel Group Corporation

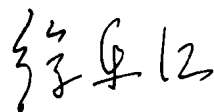
# 前 言

首届宝钢学术年会(Baosteel AAC'04)于2004年5月27~28日在上海宝钢召开。这是宝钢第一次举办这样的开放式、大型国际学术交流会。中国钢铁市场及钢产量的快速增长已成为举世瞩目的焦点,宝钢作为中国最大的钢铁制造企业,在中国和世界钢铁工业的舞台上扮演着重要的角色。我们希望通过积极认真地举办宝钢学术年会,搭建起世界钢铁科技进步的交流平台,为推动世界钢铁业的技术进步和可持续发展作出更积极、更有价值的努力和贡献。

全球钢铁工业的快速发展引发了一系列“能源”、“资源”和“环境”等方面的问题。如何正确理解和实施科学发展观,是宝钢长期以来十分重视和致力去完成任务,我们也有着较多的认识和实践,我们将本届年会的主题定为:“可持续的钢铁,可持续的未来”。宝钢十分愿意面向世界,博采众长,加强技术交流与协作,坚持可持续发展观念,共同推动冶金科技进步。

非常感谢国内外广大专家学者对本届学术年会的大力支持和热情参与,也非常感谢宝钢内外的广大科技工作者在较短时间内为大会提供大量高水平、有价值、有影响力的学术论文。对于来自国内外的430篇论文,我们组织专家认真筛选,确定170余篇结集出版。本《论文集》共五册,包括主题报告分册、碳钢生产工艺技术及其产品研发(第一册)、冶金设备及自动控制(第二册)、节能技术、环保和可持续发展(第三分册)、不锈钢和特殊钢生产工艺及其产品研发(第四分册)。希望我们的工作能得到广大科技工作者的理解和肯定。特别感谢本届年会学术委员会成员和顾问专家们为大会成功召开所做的努力和贡献,衷心感谢本届年会的筹备人员和本《论文集》编辑人员所做出的努力。

由于时间和水平有限,《论文集》中疏漏与错误难免,恳请读者批评指正。



2004年5月

## 《宝钢学术年会论文集》编委会

主 编：崔 健

编 委：(按姓氏笔画为序)

王 喆 王承学 方 园 朱立新 华建新

刘 晓 孙全社 杜 斌 李维国 邹 宽

吴东鹰 余永桂 张永杰 张清朗 陆匠心

陆祖英 陈 静 陈英颖 俞盘潮 施胜洪

徐明华 盛更红 崔 健 龚 斌 薛祖华

责任编辑：翁国强 刘宏娟

# 目 次

1	High nitrogen austenitic stainless steels for sustainable development .....	Markus O. Speidel( 1 )
2	钢的加热冷却过程的数值模拟 .....	潘健生等( 9 )
3	中国不锈钢冶炼工艺技术的进展 .....	林企曾等( 16 )
4	Baosteel group special steel's competitive edge in globalization .....	Xie Wei( 23 )
5	Tendency analysis of the Chinese stainless steel market and competitive advantages of Shanghai No.1 steel company of Baosteel group .....	Fu Zhongzhe( 31 )
6	国内冷轧不锈钢市场及宝新对策 .....	刘 安( 38 )
7	氮在不锈钢中的作用及其在冶炼和凝固过程中的控制 .....	姜周华等( 43 )
8	中国特殊钢企业产品和工艺结构调整探讨 .....	董 瀚( 48 )
9	Modification of 1000MPa grade high strength non-quenched bainitic steel for plastic mould .....	Jiang Laizhu <i>et al</i> ( 53 )
10	热作模具钢 SWPH13 的生产 .....	徐明华等( 57 )
11	电弧炉热装铬铁水冶炼不锈钢母液动态模型的研究 .....	李 青等( 62 )
12	超纯轴承钢的工艺研究 .....	虞明全等( 68 )
13	热卷箱技术及其在不锈钢带钢生产中的应用 .....	黄俊霞等( 73 )
14	Effect of composition on mechanical properties of near $\alpha$ type Ti-alloys for ships .....	Mao Pengling( 78 )
15	热处理对低层状析出气阀钢 LF6 性能的影响 .....	程世长等( 82 )
16	VD 冶炼轴承钢时渣中 CaO 还原热力学分析 .....	陈秀娟等( 89 )
17	Numerical modeling of growth kinetics of pro - eutectoid ferrite transformed from austenite in Fe - C - $\Sigma$ X alloys .....	Liu Zhen yu <i>et al</i> ( 93 )
18	T91 高压锅炉管的研制与应用 .....	王起江等( 99 )
19	热模/等温精密锻造技术的发展 .....	庞克昌(105)
20	热处理工艺对 10NiMnCrMoCu 钢组织性能的影响 .....	施荣华等(109)
21	含 Cr > 25 % 合金母液二步法冶炼方案中熔化还原竖炉行为的数学模拟 .....	王成善等(115)
22	超高强钢 23Co14Ni12Cr3 韧性的改善 .....	王六定等(120)
23	Ferrite formation on MnS in non heat-treated steel from ingot .....	Yin Jiang(125)
24	软磁结构钢热加工形变行为的研究 .....	刘自成等(129)
25	硼在 GH4049 合金晶界中的作用 .....	陈国胜等(134)
26	在 DHCR 条件下不锈钢和碳钢热轧混合轧制的研究 .....	杨建中等(139)
27	航空航天用超高强度钢的现状与发展 .....	张景海等(144)
28	保护气氛电渣重熔高温合金的冶金质量 .....	金 鑫等(148)
29	不锈钢热轧钢带生产标准的研讨 .....	叶晓宁(152)
30	高精度膨胀合金带钢的技术与工艺 .....	黄 剑等(157)
31	海洋采油平台钢板的研究 .....	金 涛等(164)
32	缆索用高强度 PC 镀锌钢丝的研制生产 .....	桑春明等(169)
33	高氮奥氏体不锈钢的试验研究 .....	陈志强(173)
34	New concepts in stainless steel technology on the base of hot metal and conarc - process .....	J. Reichel <i>et al</i> (177)

## High Nitrogen Austenitic Stainless Steels for Sustainable Development

Markus O. Speidel

(Swiss Academy of Material Science, Birmenstorf, Switzerland

Central Iron and Steel Research Institute, Beijing China)

**Abstract:** Nitrogen can replace nickel in austenitic stainless steels, thus resulting in products which are: more environmentally benign through conserving resources; more economic due to the low cost of nitrogen; much stronger in the extreme up to 3600MPa; much more ductile than other steels of the same strength; more corrosion resistant for one weight percent nitrogen equals twenty percent of chromium in terms of localized corrosion resistance; more stress corrosion cracking resistant; biocompatible not causing nickel allergy. These advantages, taken together, will make high nitrogen austenitic stainless steel prime candidate material for the future sustained development and for products which last longer and can do more with less. The disadvantages of the steel include limited weldability; and the specific manufacturing process. High nitrogen austenitic stainless steel already exists as niche products and has been made on an industrial scale in various product forms. A wide application is expected with the mastering of the processing technologies for large - scale production. Potential products are outlined from the point of view of a sustained development where conserving of resources, low cost, high strength, high toughness and high corrosion resistance of steels are required. For the startup of this sustainable development, existing production equipment can be used.

**Key Words:** High nitrogen steel; austenitic stainless steel; strength and ductility; strength-to-density ratio; sustainable development

### 1 Introducing nitrogen into solid solution

One of the most pronounced and most useful effects of nitrogen in iron solid solutions is the stabilization of the face centered cubic crystal lattice, as seen in Figure 1 for steels with 23 weight percent chromium. This effect is fully made use of in austenitic high nitrogen steels, but quenching is always necessary to retain the austenitic phase at ambient temperature. Therefore, the introduction of enough nitrogen into the steel during processing and its retention in solid solution during heat treatment require specific know-how for the steelmaker. This know-how is presently being established in China by pilot production.

### 2 Strength and ductility

Nitrogen in solid solution affects at least four strengthening mechanisms positively: solid solution hardening, grain refinement hardening, work hardening and strain aging<sup>[1-5]</sup>. Thus, any discussion on the strength of high nitrogen austenitic steel needs to con-

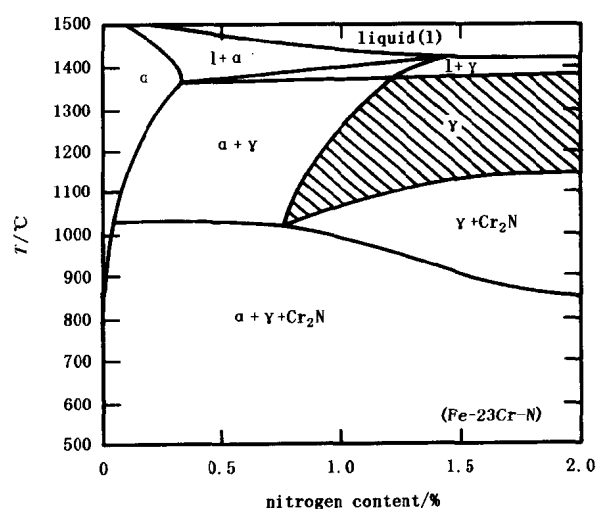


Fig. 1 Nitrogen in solid solution gives rise to fcc phase stability for iron base alloys with 23 weight-percent chromium. Without nitrogen, such alloys would never be even potentially austenitic, but very stable ferritic

sider the effect of grain size is to be of academic value or of practical value. An example of the effect of grain

size is shown in Figure 2. Note that the yield strength can vary from less than 600 to more than 1 200 MPa.

The three equations contained in Figure 3 are the modified Hall-Petch equations for yield strength,  $R_{p0.2}$ , ultimate tensile strength,  $R_m$ , and elongation to frac-

ture,  $A_5$ . The data in Figure 4 indicate that a metallurgist's dream has come true: nitrogen in solid solution increases the strength and the ductility at the same time.

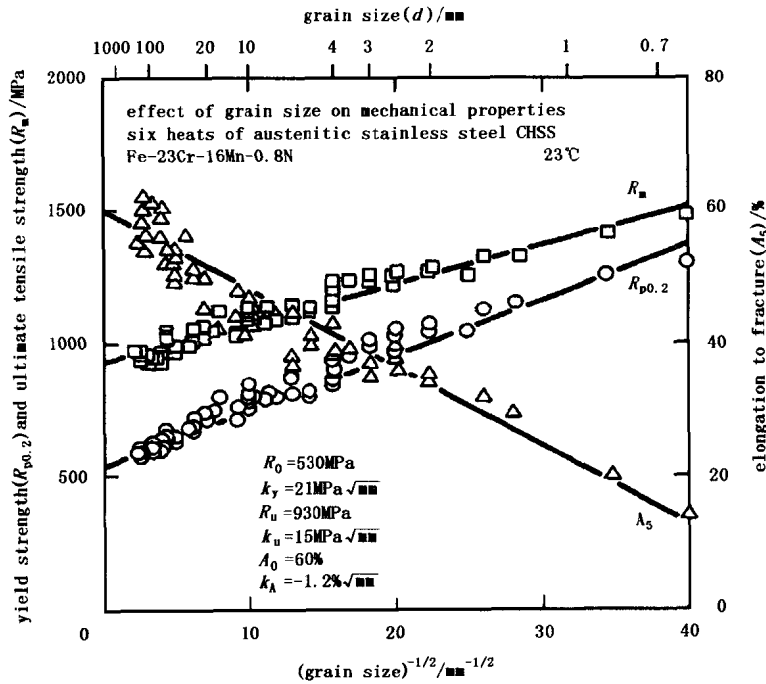


Fig.2 Effect of grain size on strength and ductility

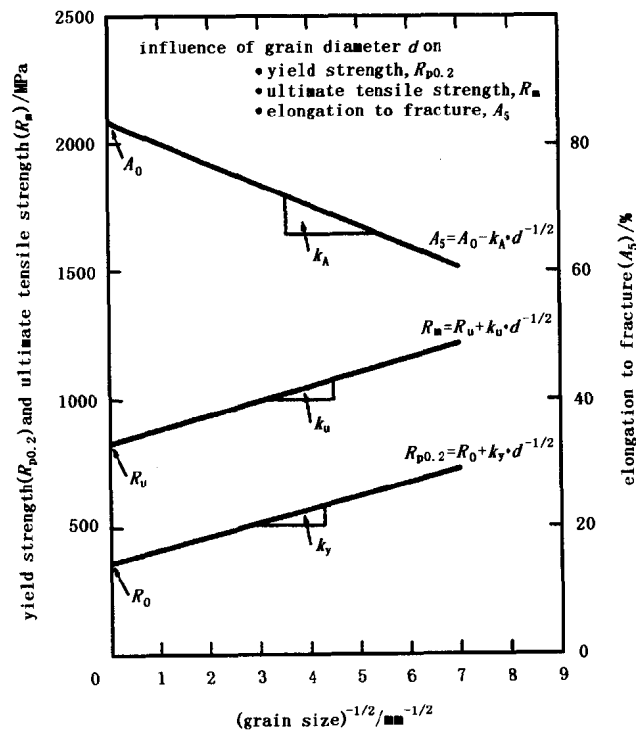


Fig.3 Schematic defining the mechanical properties relating to the grain size

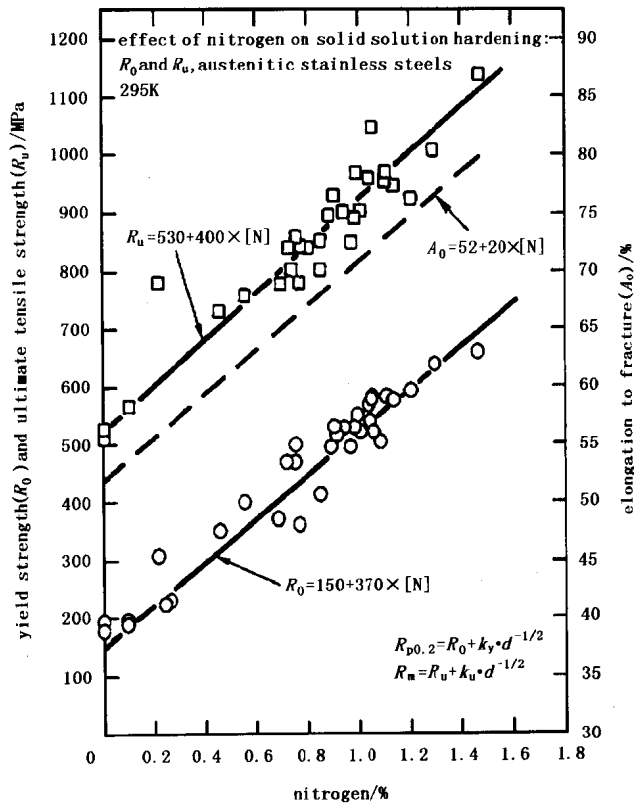


Fig.4 Nitrogen in solid solution enhances strength and ductility at the same time

Cold work is one of the most effective ways to increase the strength of high nitrogen austenitic steels, as indicated in Figure 5; higher nitrogen contents in solid solution result in higher work hardening coefficients. With a sufficient degree of cold work, this can lead to extremely high strength values. So far, we have obtained 3600MPa, Figure 6, and there is no theoretical reason why this could not be pushed beyond 4 000 MPa in the near future.

Strength alone is not the goal for the development of structural materials. Rather, the combination of strength and ductility, as shown in Figure 7, or the combination of strength and fracture toughness, as shown in Figure 8, must be the goal, as this is what the designer needs. Consider, for example, steels for modern cars; they require strength in order to be lightweight and thus fuel efficient for a sustainable economy. They require also ductility for two reasons: for energy absorption during a crash, and thus crash safety, and for good formability during production of components, for example by internal high pressure forming. It is quite clear from Figure 7 that high nitrogen austenitic steels are by far superior to the ferritic steels presently used for car

making (with a yield strength less than 1 000 MPa) when compared at equal ductility or when compared at equal strength.

A closer inspection of the strength and fracture toughness data in Figure 8 has shown that high nitrogen austenitic steels not only exhibit the highest combination of strength and fracture toughness of all steels, but of all materials in the world: there is no material which shows a higher product of strength and fracture toughness than high nitrogen austenitic stainless steels.

For many applications materials are needed which have a high strength to density ratio. This is critical for the light weight structures of a future sustainable development. Examples are not only cars, but everything that moves, including trains, ships, airplanes, rockets, and also rotating components. We therefore show in Figure 9 the ductility of presently used car sheet steels as a function of their strength to density ratio. Compared with the car sheets are their alternative materials made of Al, Mg, Ti, and high nitrogen austenitic steels. It is clear that high nitrogen austenitic steels are superior not only to presently used car steels, but also to Al, Mg, and even Ti!



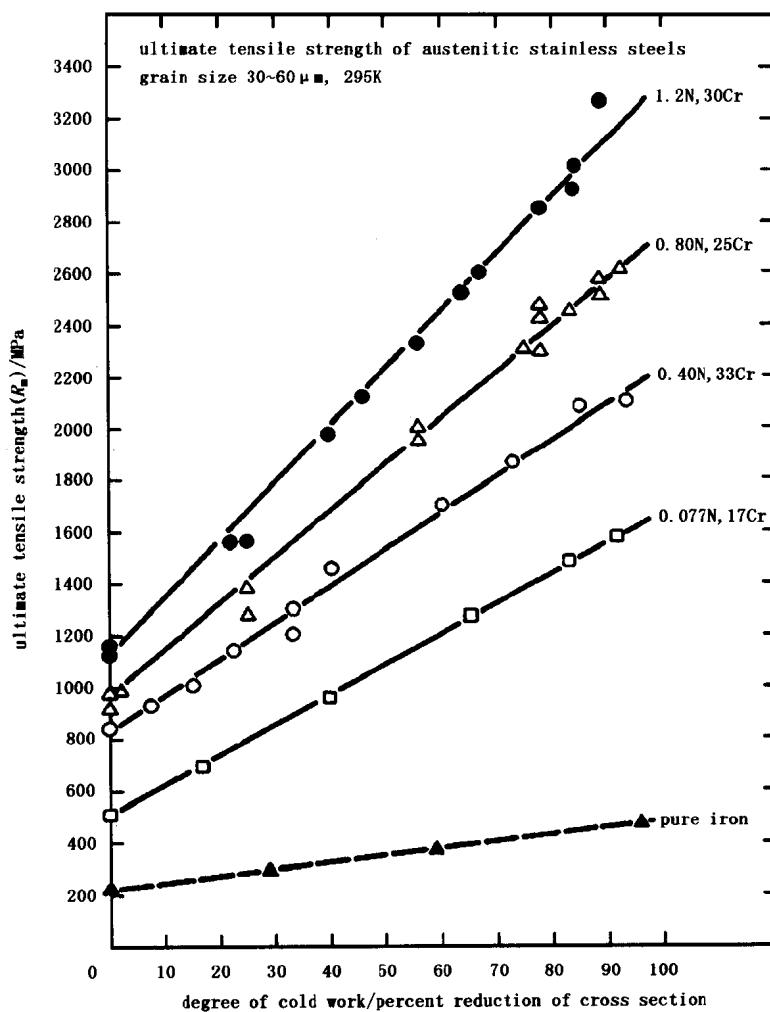


Fig.5 Nitrogen in solid solution strongly enhances work hardening

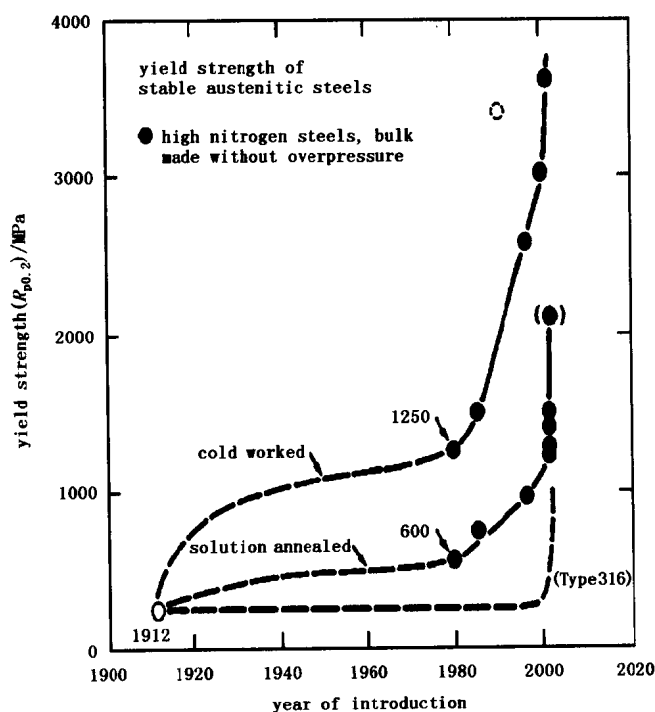


Fig.6 Austenitic steels with extreme strength levels have been realized

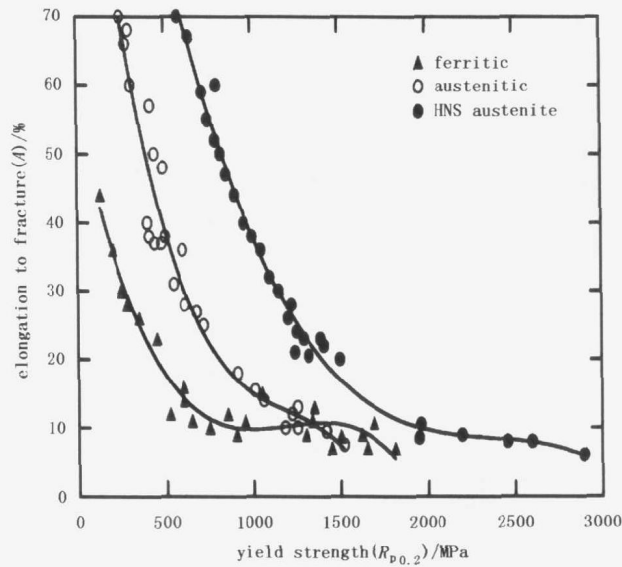


Fig.7 Ferritic steels, as used for cars and armor, compared with austenitic steels

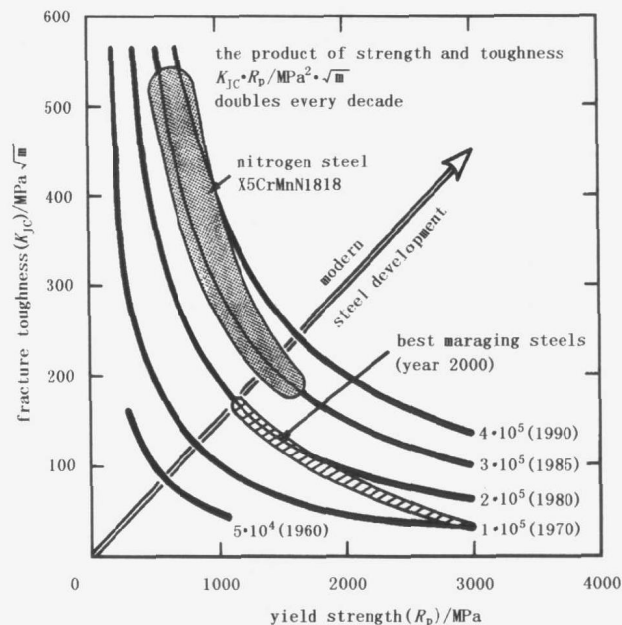


Fig.8 Of all the steels presently available, high nitrogen austenitic steels exhibit the highest combination of strength and fracture toughness

Under triaxial stresses and impact loading, such as Charpy V-notch tests, very high nitrogen containing austenitic steels can fail in a brittle manner, as shown in Figure 10. The failure mechanism is glide band separation along  $\{111\}$  planes of the fcc crystal lattice. This puts an upper limit to the useful nitrogen additions in high nitrogen austenitic steels.

### 3 Corrosion resistance

Nitrogen in solid solution increases the resistance

of austenitic stainless steels to general corrosion, pitting corrosion and crevice corrosion. The resistance to pitting and crevice corrosion depends on the alloy composition according to the following correlation equation:

$$\text{MARC} = \text{Cr} + 3.3\text{Mo} + 20\text{C} + 20\text{N} - 0.5\text{Mn} - 0.25\text{Ni}$$

where MARC stands for measure of alloying for resistance to corrosion and the elements symbols stand for the alloying content of each element in weight percent. The MARC correlation has been found applicable to

both commercial and experimental austenitic stainless steels, as seen in Figure 11 and Figure 12. It is thus a very valuable tool in alloy design. At this time there is no fundamental justification or explanation for MARC available. The one most remarkable fact here is, howev-

er, that within the limits of the austenitic stainless steels investigated so far, one weight percent nitrogen confers as much corrosion resistance as 20 weight percent chromium.

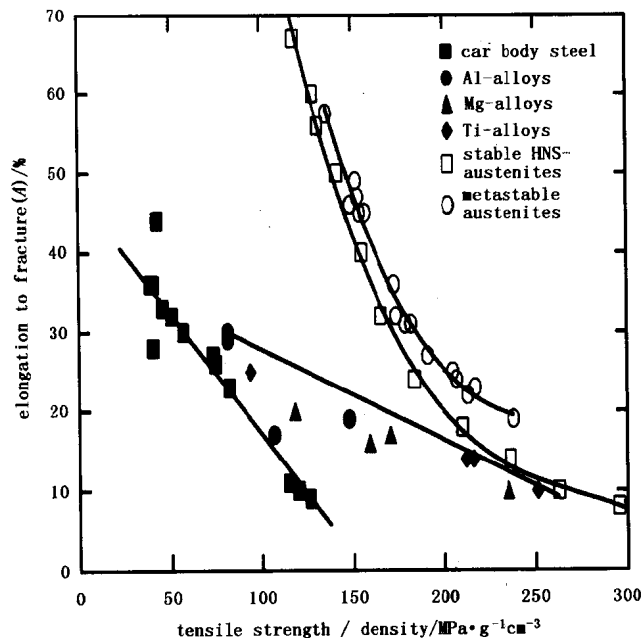


Fig.9 At equal ductility, high-nitrogen austenitic steels are superior in strength to density not only to car sheet steels, but also to Al-, Mg-, and Ti- base alloys

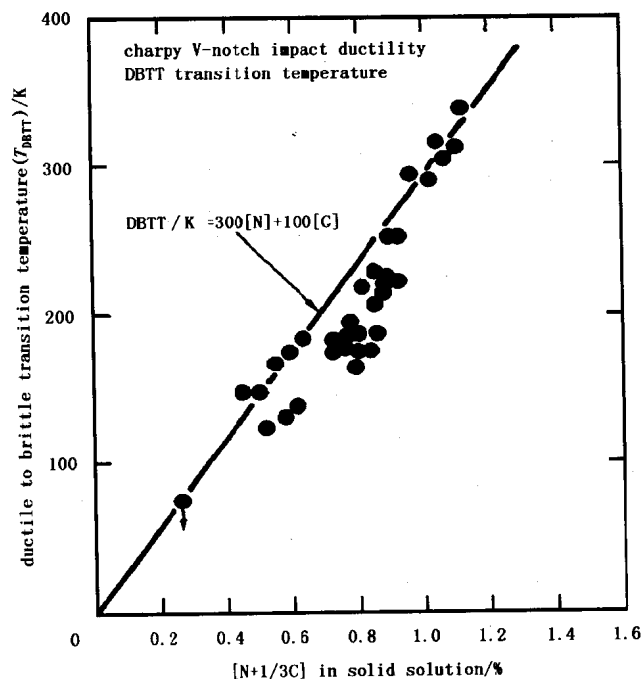


Fig.10 DBTT as a function of nitrogen. Extreme nitrogen contents render austenites brittle

Stress corrosion cracking in hot concentrated chloride solutions is one of the well known weaknesses of the austenitic stainless steels. Thus, it may be seen in

Figure 13 that both Type 304 and Type 316 austenitic stainless steels exhibit readily stress corrosion cracking in 22% NaCl solutions at 105°C. In contrast, our high

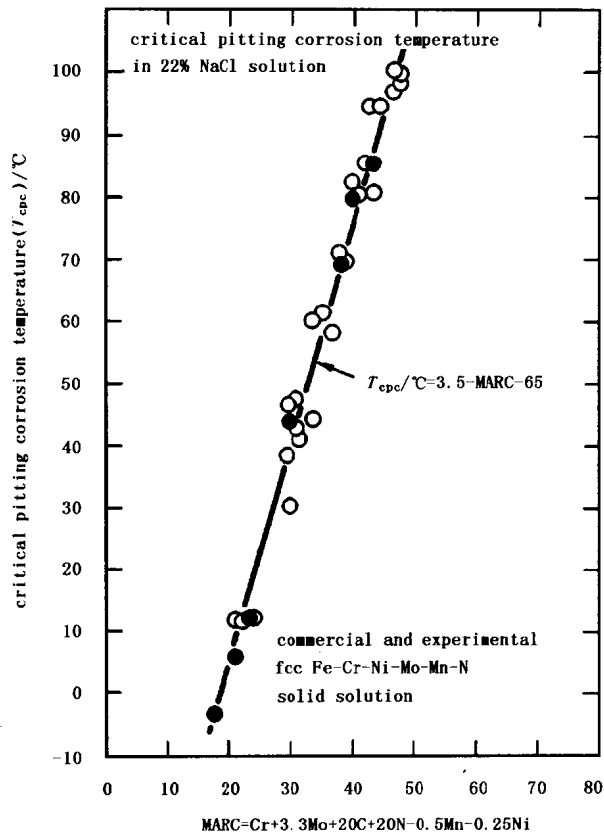


Fig. 11 The critical pitting corrosion temperature, and thus the resistance to pitting corrosion, depends on the alloy composition according to the MARC correlation

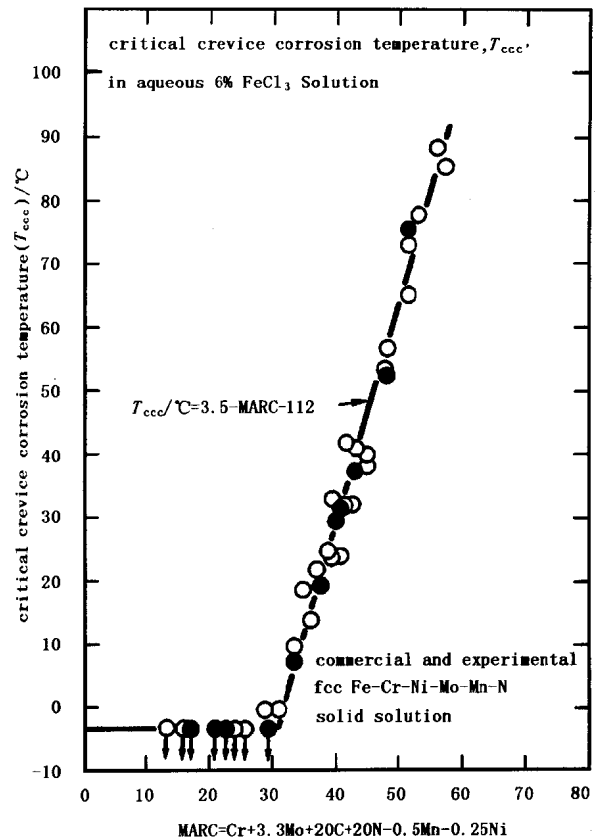


Fig. 12 The critical crevice corrosion temperature and thus the resistance to crevice corrosion depends on the alloy composition according to the MARC correlation

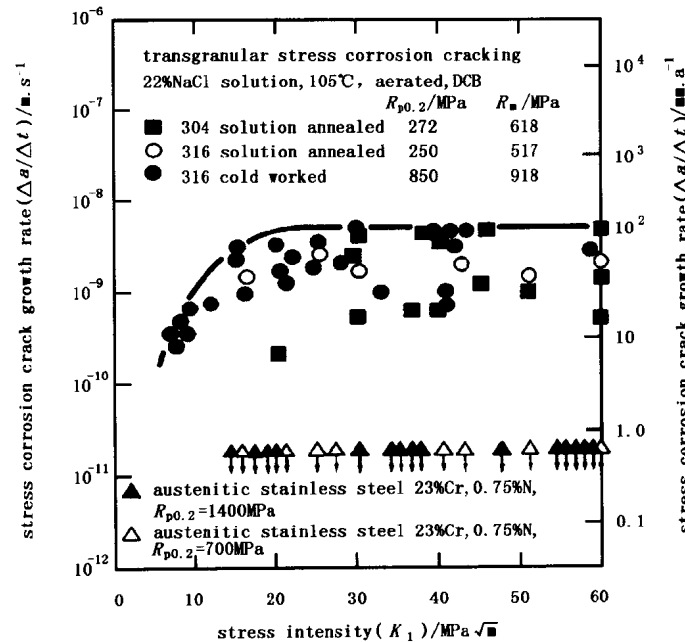


Fig. 13 Growth rates of stress corrosion cracks in austenitic stainless steels with 23 percent chromium are much more resistant- say, immune- to chloride induced stress corrosion cracking at 105°C where both Type 304 and 316 austenitic stainless steels fail readily

nitrogen austenitic stainless steels resist such cracking even when cold worked up to a strength level of 1 400 MPa.

#### 4 Applications

High nitrogen stainless steels have been made in industrial quantities for many years, but only as niche products i. e. for very specific applications of high added value. Therefore, the production methods could be expensive and often included pressure metallurgy, such as pressurized electroslag remelting. Because of the high quality of the products so obtained, this production method will continue and expand in the future. However, quite recently we have developed methods to make high nitrogen steels with existing equipment for large scale production such as NOD and continuous casting and/or ingot casting. While improvements are still desirable, it is now clear that high nitrogen stainless steels are ready for mass production as well as for small scale high quality production.

The properties outlined above, as well as further advantageous properties which space does not permit to outline here, will make high nitrogen stainless steels strong candidate materials for applications in the trans-

portation industry (cars, railroads, ships), in the building industry (fixations, rebars for the general salvation of our corroding infrastructure such as bridges and tunnels) in the aerospace industry, in ocean engineering, in the sports goods industry, and even in the nuclear power industry and the military.

Because of their high strength, ductility and corrosion resistance high nitrogen steels can do more with less material and products made of them will have greatly extended useful service duration. These are the hallmarks of steels for sustainable development.

#### References

- 1 H. J. C. Speidel and M. O. Speidel, *Materials and Manufacturing Processes*, 2004; 19: 95
- 2 M. O. Speidel, *Zeitschrift Metallkunde*, 2003; 94: 119
- 3 M. O. Speidel, M. L. Zheng. in the book of HNS 2003 High Nitrogen Steels, vdf Hochschulverlag ETH Zurich, Switzerland, 2003: 63 ~ 73
- 4 H. J. C. Speidel and M. O. Speidel, *ibid*, 101 ~ 112
- 5 M. O. Speidel. Ultra high strength austenitic stainless steels. *Stainless Steel, World Conference 2001, The Hague, The Netherlands, November 2001*
- 6 M. O. Speidel. *Proceedings of ICASS 2004, Shanghai*, 761 ~ 767
- 7 M. O. Speidel *et al.* *Trans. Indian Inst. Met.*, 2003; 56: 281
- 8 M. O. Speidel. *CAMP-ISIJ*, 2000; 13: 372

## 钢的加热冷却过程的数值模拟

潘健生, 顾剑锋

(上海交通大学 材料科学与工程学院)

**摘要:**文章阐述了钢的加热和冷却过程的数学模型。数值模拟中用增量叠代法处理边界条件非线性、物性参数非线性、相变潜热非线性等复杂的非线性问题。在相变量计算中引入应力状态的影响。在应力场分析中建立了采用热弹塑性模型,考虑了相变应变、相变塑性应变、热应变、材料机械性能的温度效应和相变影响等因素。通过模拟可以获得钢件内部任意位置的加热和冷却曲线,直观显示出任一时刻的瞬态温度场、组织分布和应力场。结合已经进行的研究工作的具体实例,论证了钢的加热和冷却过程的数值模拟是一种极具实际应用价值的虚拟生产试验的手段,可以作为智能热处理的核心技术之一。

**关键词:**加热;淬火;相变;温度场;应力场;有限元法;数值模拟

### Numerical Simulation of Heating and Cooling Process of Steel

PAN Jian-sheng GU Jian-feng

(Shanghai Jiaotong University School of Materials Science and Engineering)

**Abstract:** In this paper, the mathematical model for heating and cooling process of steels has been discussed in details. During numerical simulation, the incremental iteration method is used to deal with such complicated nonlinear as boundary nonlinear, physical property nonlinear, transformation nonlinear etc. The effect of stress state on transformation has been considered in the calculation of microstructure. In the stress field analysis, a thermo-elastic-plastic model has been founded, which considers such factors as transformation strain, transformation plastic strain, thermal strain and the effect of temperature and transformation on mechanical properties etc. By means of simulation, the heating and cooling curve on any position of steel parts can be obtained, and the transient temperature field, microstructure distribution and stress field at any time can be displayed vividly. Combining with the specific examples, it is demonstrated that the simulation of heating and cooling process of steels is an excellent practical approach of virtual manufacture technique, which acts as one of the core technology of intelligent heat treatment.

**Key Words:** Heating; Quenching; Phase transformation; Temperature field; Stress field; Finite element method (FEM); Numerical simulation

#### 1 前言

加热工艺是热处理的一个重要环节,合理选择加热工艺对节能具有重要意义。加热的节能主要是如何合理地切合实际地选择加热时间和缩短保温时间。人们在这方面开展了很多工作,取得了一些经验性公式。但目前关于热处理加热时间的计算仍无一个完善统一的方法,因此传统选择加热工艺的方法具有很大的局限性。计算机数值模拟技术具有坚实的科学基础,它综合传热学、奥氏体化相变动力学理论,运用有限元数值分析方

法可得到热处理过程任一瞬时工件内部温度场分布和组织分布,可以精确预测透烧情况下所需的加热时间,实现“零保温”工艺。

淬火是钢热处理中最为广泛的工艺。机械零件和工模具在淬火过程中产生的内应力造成变形、开裂,是工业上普遍存在的问题。由此造成的材料、能源、工时的损失不可低估。在淬火冷却这个复杂的物理过程中,温度场、组织场和应力场都在连续不断地变化着,三者互相联系、互相影响,不可分割<sup>[1]</sup>。建立耦合的数学模型是热处理领域

世界范围内的热点和最新成果<sup>[2,3]</sup>。温度场、组织场和应力场的耦合关系相当复杂,牵涉面广,需要结合三维温度场传热计算<sup>[4]</sup>、相变动力学计算<sup>[5]</sup>、有限元数值方法和热弹塑性力学等其它学科的研究成果。

## 2 加热和冷却过程的数学模型

### 2.1 加热过程的数学模型

#### 2.1.1 含相变潜热的非线性瞬态温度场

考虑相变潜热的三维非线性导热偏微分方程在直角坐标下的形式为:

$$\rho c \frac{\partial T}{\partial t} = \frac{\partial}{\partial x} \left( k \frac{\partial T}{\partial x} \right) + \frac{\partial}{\partial y} \left( k \frac{\partial T}{\partial y} \right) + \frac{\partial}{\partial z} \left( k \frac{\partial T}{\partial z} \right) + Q \quad (1)$$

其中,  $k$  为导热系数,  $\rho$  为密度,  $c$  为比热容,  $Q$  为相变潜热。在求解瞬态温度场时,需要相应的初始条件和边界条件。初始条件是指待求的非稳态传热问题在初始时刻整个区域中各点温度值是已知的,它可以是常值,也可以是空间坐标的函数,如下式。

$$T|_{t=0} = T_0 \text{ 或 } T|_{t=0} = T_0(x, y, z) \quad (2)$$

$t$  表示传导时间,  $T_0$  为已知常数,若物体初温是不均匀的,则  $T_0$  表示已知函数。

边界条件有以下几类:  $S_1$ ——温度已知,  $S_2$ ——边界热流已知,  $S_3$ ——对流边界加辐射边界。

$$\text{综合表示边界条件为: } k_x \frac{\partial T}{\partial x} l_x + k_y \frac{\partial T}{\partial y} l_y + k_z \frac{\partial T}{\partial z} l_z - q + h_\Sigma (T - T_\infty) = 0 \quad (3)$$

$$h_\Sigma = h_c + h_R \quad (4)$$

式中,  $l_x, l_y, l_z$  为方向余弦;  $q$  为  $S_2$  边界上的热流通量,  $T_\infty$  为环境温度,  $h_\Sigma$  为  $S_3$  边界上的综合换热系数,  $h_c$  为对流换热系数,  $h_R$  为辐射换热系数。(1)式中的内热源项  $Q$  来自相变潜热,这些潜热对温度场分布影响较大,不能忽略。

$$Q = \Delta H \cdot \frac{\Delta V}{\Delta t} \quad (5)$$

式中,  $\Delta H$  为生成单位体积奥氏体时吸收的热量,取平均值  $-6.0 \times 10^8 \text{ J/m}^3$ ,  $\Delta V$  为在时间  $\Delta t$  内的奥氏体生成量。

#### 2.1.2 奥氏体生成量的计算

加热奥氏体化过程是一个扩散型转变的过程,加热的原始组织简单地称为非奥氏体组织,当温度上升达到  $A_{c1}$  点以后,开始计算孕育期累加;

当孕育期累加达到 1 时,开始计算奥氏体生成量。加热奥氏体生成几乎是淬火过程中奥氏体分解的逆过程(不包括马氏体转变),后者的计算在一些文献中讨论比较多<sup>[6~8]</sup>。

在孕育期的计算中,运用孕育期累加法来判断相变是否开始发生。孕育期累加值大于 1 则相变开始发生;累加值小于 1,则继续进行孕育期累加。

$$\sum_{i=1}^n \frac{\Delta t_i}{\tau_{iTTA}} = 1 \quad (6)$$

式中,  $\Delta t_i$  是微小等温时间段,  $\tau_{iTTA}$  为完全奥氏体化所需的时间。

对于扩散型转变,转变量的计算利用 Avrami 等人提出的转变量—时间 ( $V-t$ ) 公式:

$$V = 1 - \exp(-bt^n) \quad (7)$$

式中,  $V$  为奥氏体生成量,  $t$  为等温时间,  $b$  和  $n$  为与转变动力学有关的常数。

### 2.2 淬火过程的数学模型

淬火过程也就是温度场、组织场和应力场相互作用的过程,淬火过程的综合数学模型由三个方面的内容组成。

#### 2.2.1 温度场分析

三维温度场传热控制偏微分方程:

$$\rho c \frac{\partial T}{\partial t} = \frac{\partial}{\partial x} \left( k \frac{\partial T}{\partial x} \right) + \frac{\partial}{\partial y} \left( k \frac{\partial T}{\partial y} \right) + \frac{\partial}{\partial z} \left( k \frac{\partial T}{\partial z} \right) + Q_1 + Q_2 \quad (8)$$

式中,  $\rho$  为密度,  $c$  为比热容,  $k$  为导热系数, 内热源项  $Q_1$  和  $Q_2$  分别代表相变潜热和塑性功生成热:

$$Q_1 = \Delta H \cdot \frac{\Delta V}{\Delta t} \quad Q_2 = Mf \frac{dW^p}{dt} \quad (9)$$

其中  $dW^p = \sigma_{ij} \cdot d\epsilon_{ij}^p$

式中,  $\Delta H$  为发生单位体积奥氏体分解时释放的热量,  $\Delta V$  为在  $\Delta t$  时间内奥氏体分解的体积,  $M$  为热功当量,  $f$  为塑性功转化为热量的百分数,  $W^p$  为塑性功,  $\sigma_{ij}$  为应力张量,  $\epsilon_{ij}^p$  为塑性应变张量。

淬火边界条件为对流和辐射换热,采用合并的格式:

$$\text{对流换热热流密度 } Q_{s1} = h(T_r - T_s);$$

$$\text{辐射热流密度 } Q_{s2} = K_r(T_r - T_s),$$

$$\text{其中 } K_r = \epsilon p \sigma_0 (T_r^2 + T_s^2)(T_r + T_s).$$

式中,  $h$  为换热系数,  $\epsilon$  为黑度系数,  $T_r$  为工件表面温度,即辐射源温度,  $T_s$  为介质温度,  $p$  是与两辐射物体形状有关的平均角系数,称形状因

子,  $\sigma_0$  为 Stefan-Boltzmann 常数 ( $\sigma_0 = 5.67 \times 10^8 \text{ W}/(\text{m}^2 \cdot \text{K}^4)$ )。

总的热流密度为:

$$Q_s = Q_{s1} + Q_{s2} = (K_r + h)(T_r - T_s) \cdots \cdots (10)$$

淬火初始条件为淬火前工件内的温度场分布, 对于整体均匀透烧情况,  $T|_{t=0} = T_0$ ; 对于局部加热如感应加热等,  $T|_{t=0} = T_0(x, y, z)$ 。

### 2.2.2 组织转变计算

通过时间离散, 将连续冷却视为阶梯冷却, 对每个离散时间段的阶梯平台可按等温考虑。Scheil 运用叠加法则解决了阶梯等温作用的叠加问题。F. M. B. Fernandes 和 A. Simon、S. Denis<sup>[2]</sup> 认为相变包括形核和生长两个过程。形核期的计算采用 Scheil 的逐温孕育成核相加理论, 该理论认为: 连续冷却过程可以看成许多短暂的阶梯等温过程所组成, 每一短暂等温时间都具有短暂的孕育效果, 各次短暂孕育效果可以累积相加。设定过冷奥氏体达到分解时的效果为 1, 而某一短暂等温时间的孕育效果为  $\Delta t_i / \tau_{iIT}$ ,  $\Delta t_i$  为短暂等温时间,  $\tau_{iIT}$  为某一阶梯冷却温区的中点温度下等温转变的孕育期。当各  $\Delta t_i / \tau_{iIT}$  累积之和等于 1 时, 即认为各短暂孕育效果累积达到了成核所需的孕育期, 而过冷奥氏体开始转变。相变的计算方法如下:

$$\text{孕育期叠加法则: } \sum_{i=1}^n \frac{\Delta t_i}{\tau_{iIT}} = 1 \cdots \cdots (11)$$

$$\text{扩散型相变相变量计算: } V = 1 - \exp(-bt^n) \cdots \cdots (12)$$

$$\text{马氏体相变相变量计算: } V = 1 - \exp[-\alpha(M_s - T)] \cdots \cdots (13)$$

考虑应力状态的影响而进行修正。对扩散型相变修正系数  $b$  和  $n$ <sup>[9]</sup>:

$$\left. \begin{aligned} n_e &= n \\ b_o &= \frac{b}{(1-D)^n} \end{aligned} \right\} D = C\sigma_e \cdots \cdots (14)$$

对马氏体相变修正计算公式和  $M_s$  点<sup>[9]</sup>:

$$V = 1 - \exp[-\alpha(M_s - T) - \varphi(\sigma)] \cdots \cdots (15)$$

$$\varphi(\sigma) = A\sigma_m + B\sigma_e^{1/2} \cdots \cdots (16)$$

$$M_s = M_{s0} + \Delta M_s, \quad \Delta M_s = A\sigma_m + B\sigma_e \cdots \cdots (17)$$

以上各式中,  $V$  为奥氏体分解的转变量;  $\sigma_m$  为平均应力;  $\sigma_e$  为等效应力;  $A, B, C$  为常数;  $b, n, \alpha$  为系数;  $T$  为温度;  $t$  为时间;  $M_s$  为马氏体点。

### 2.2.3 应力场分析

淬火过程中应力应变的模拟结果以及对淬火后的残余应力和变形的预测的准确性, 与所采用的材料力学模型密切相关。目前的淬火模拟已经从原来的弹性模型改进为弹塑性模型。同时应该考虑材料的力学性能, 如加工硬化特性、塑性流动法则、屈服准则等。通常采用 Von - Mises 准则, 等向硬化条件和普朗特 - 劳埃斯 (Prandtl - Reuss) 塑性流动法则, 由这些条件可以推导出弹塑性模型本构方程:

$$d\epsilon_{ij} = \frac{1-2\mu}{E} d\sigma_m \delta_{ij} + \frac{1}{2G} dS_{ij} + \frac{3}{2H} \cdot \frac{d\sigma_i}{\sigma_i} S_{ij} \cdots \cdots (18)$$

淬火过程中应力分析, 必须考虑相变的影响, 因此塑性区的处理远远较普通的应力分析复杂。总应变应该包括弹性应变、塑性应变、热应变、相变应变和相变塑性应变等多项。

$$\text{总应变: } d\epsilon_{ij}^T = d\epsilon_{ij}^e + d\epsilon_{ij}^p - d\epsilon_{ij}^{th} + d\epsilon_{ij}^{tr} + d\epsilon_{ij}^{pp} \cdots \cdots (19)$$

$$\text{弹性应变: } d\epsilon_{ij}^e = \frac{1}{2G} dS_{ij}, \text{ 即 } d\epsilon_{ij}^e = \frac{1}{2G} d\sigma_{ij} \cdots \cdots (20)$$

$$\text{塑性应变: } d\epsilon_{ij}^p = d\lambda S_{ij}, \text{ 即 } d\epsilon_{ij}^p = \frac{3}{2H} \cdot \frac{d\sigma_e}{\sigma_e} \sigma_{ij} \cdots \cdots (21)$$

$$\text{热应变: } d\epsilon_{ij}^{th} = \sum_{k=1}^5 m_k \cdot \alpha_k(T) dT \cdots \cdots (22)$$

$$\text{相变应变: } d\epsilon_{ij}^{tr} = \sum_{k=2}^5 dV_k \cdot \beta_k^T, \beta_k^T = \beta_k^0 + (\alpha_k - \alpha_A)T \cdots \cdots (23)$$

$$\text{相变塑性应变: } d\epsilon_{ij}^{pp} = 3K\sigma_{ij}(1-V) \cdot \Delta V \cdots \cdots (24)$$

以上各式中,  $G$  剪切模量,  $H$  为加工硬化指数,  $K$  为系数 (实际上也是应力的函数),  $\epsilon_{ij}$  为总的应变张量,  $\epsilon_{ij}^p$  为塑性应变张量,  $\epsilon_{ij}^e$  为弹性应力偏张量,  $\sigma_{ij}$  为应力张量,  $S_{ij}$  为应力偏张量,  $\alpha_k$  和  $m_k$  分别为不同组织的热膨胀系数和体积百分含量 ( $k=1, 2, 3, 4, 5$  分别代表奥氏体, 铁素体, 珠光体, 贝氏体, 马氏体),  $\beta_k^T$  ( $k=2, 3, 4, 5$ ) 表示在温度  $T$  下奥氏体分解为  $k$  组织时的体积膨胀系数, 而  $\beta_k^0$  则为  $0^\circ\text{C}$  下的转变膨胀系数。

### 3 数值模拟实现方法

目前, 还没有成熟完善的专门用于热处理 (钢的加热和冷却) 过程的有限元分析软件, 因此数值模拟大多基于大型通用有限元软件包, 我们的工



作是以这些通用有限元软件包 (MSC. MARC, ANSYS, ABAQUS, FPÉG 等) 为平台, 结合针对上述数学模型的特殊性而开发的嵌入式子程序来实现数值模拟。

热处理数学模型中涉及多种非线性, 非线性主要包括: (1) 材料非线性: 材料热物性参数和力学性能参数随温度变化、随着相成分而变化的材料非线性以及在应力分析中弹塑性材料的本构关系非线性 (亦即应力与应变之间非线性关系)。(2) 边界条件非线性: 表面换热系数的非线性、相变潜热非线性和塑性功生成热非线性。非线性问题的处理是难点和关键。图 1 是以增量迭代法来

求解淬火过程中耦合的温度场、组织场和应力场的计算流程示意图。

此外, 在有限元网格划分、时间步长选择及收敛判据选择都需要大量的尝试, 以选取最佳的方案, 精简计算量, 提高计算精度。

## 4 算例

### 4.1 冷轧辊的加热过程模拟

以 9Cr2Mo 冷轧辊为例, 模拟其加热过程。轧辊的形状尺寸如图 2, 在进行有限元分析时的网格如图 3 所示。应用美国 MSC. MARC 公司的大型有限元分析通用软件对前述数学模型进行模拟。通

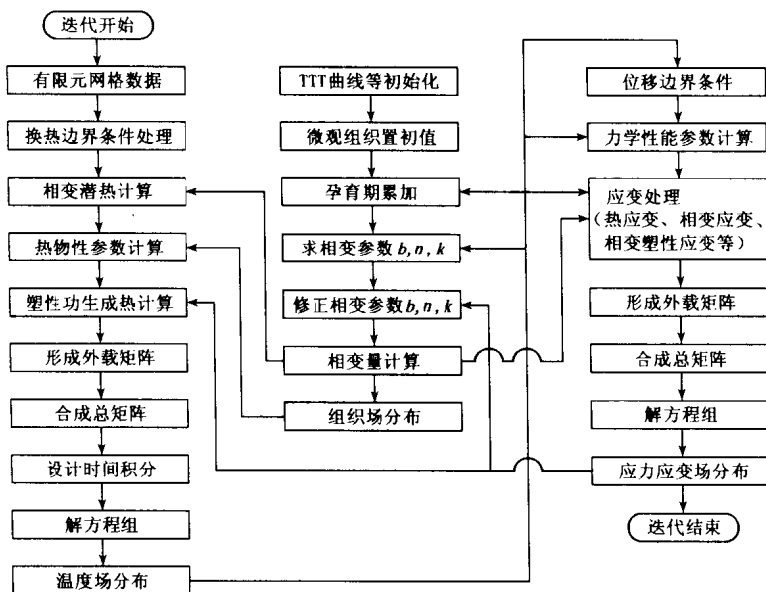


图 1 淬火应力场分析中有限元耦合计算示意图

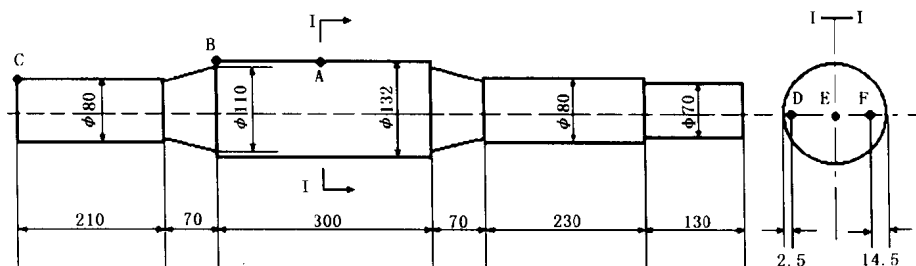


图 2 冷轧辊试样尺寸及热电偶位置 (热电偶 D、E、F)

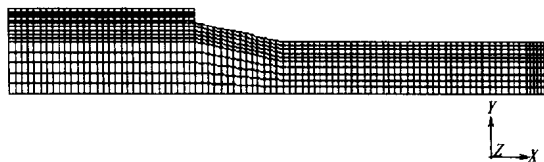


图 3 9Cr2Mo 冷轧辊的有限元网格

过分析得到了加热过程中温度场和奥氏体化的详

细的变化进程, 并输出直观的图形。图 4 为加热 5 min 和 44 min 时轧辊内部的温度场, 图 5 为加热 42 min 和 52 min 时轧辊内部的奥氏体分布。

模拟计算可以得到在轧辊上任意点的温度变化情况以及整个轧辊上的温度分布。在加热整个过程中, 在中截面上心部 E 点发生奥氏体化时, 它与表面 A 点的温差达到最大, 为 30℃ (见图 6-a); A